The Journal of Immunology

Inositol-Triphosphate 3-Kinase C Mediates Inflammasome Activation and Treatment Response in Kawasaki Disease

Martin Prince Alphonse, Trang T. Duong, Chisato Shumitzu, Truong Long Hoang, Brian W. McCrindle, Alessandra Franco, Stéphane Schurmans, Dana J. Philpott, Martin L. Hibberd, Jane Burns, Taco W. Kuijpers and Rae S. M. Yeung

J Immunol 2016; 197:3481-3489; Prepublished online 30 September 2016;
doi: 10.4049/jimmunol.1600388
http://www.jimmunol.org/content/197/9/3481

The Journal of Immunology is published twice each month by
The American Association of Immunologists, Inc.,
1451 Rockville Pike, Suite 650, Rockville, MD 20852

Print ISSN: 0022-1767 Online ISSN: 1550-6606.

Inositol-Triphosphate 3-Kinase C Mediates Inflammasome Activation and Treatment Response in Kawasaki Disease

Martin Prince Alphonse,*,† Trang T. Duong,† Chisato Shumitzu,‡ Truong Long Hoang,§ Brian W. McCrindle,¶ Alessandra Franco,‡ Stéphane Schurmans,‖ Dana J. Philpott,* Martin L. Hibberd,§ Jane Burns,‡ Taco W. Kuijpers,# and Rae S. M. Yeung*,†,¶

Kawasaki disease (KD) is a multisystem vasculitis that predominantly targets the coronary arteries in children. Phenotypic similarities between KD and recurrent fever syndromes point to the potential role of inflammasome activation in KD. Mutations in NLRP3 are associated with recurrent fever/autoinflammatory syndromes. We show that the KD-associated genetic polymorphism in inositol-triphosphate 3-kinase C (*ITPKC*) (rs28493229) has important functional consequences, governing ITPKC protein levels and thereby intracellular calcium, which in turn regulates NLRP3 expression and production of IL-1β and IL-18. Analysis of transcript abundance, protein levels, and cellular response profiles from matched, serial biospecimens from a cohort of genotyped KD subjects points to the critical role of ITPKC in mediating NLRP3 inflammasome activation. Treatment failure in those with the high-risk *ITPKC* genotype was associated with the highest basal and stimulated intracellular calcium levels and with increased cellular production of IL-1β and IL-18 and higher circulating levels of both cytokines. Mechanistic studies using Itpkc-deficient mice in a disease model support the genomic, cellular, and clinical findings in affected children. Our findings provide the mechanism behind the observed efficacy of rescue therapy with IL-1 blockade in recalcitrant KD, and we identify that regulation of calcium mobilization is fundamental to the underlying immunobiology in KD. ***The Journal of Immunology*, 2016, 197: 3481–3489.**

Kawasaki disease (KD) is a multisystem vasculitis that predominantly targets the coronary arteries in infants and young children (1). KD is characterized by prolonged fever and multisystem inflammation with polymorphous skin rash, oral mucosal changes (red, cracked lips and strawberry tongue), nonpurulent conjunctival injection, extremity changes (redness and swelling), and cervical lymphadenopathy. Epidemiological data suggest an environmental trigger with genetic factors contributing to susceptibility and severity of the disease (2, 3). Agnostic approaches to interrogate the genome have identified inositol-triphosphate 3-kinase C (*ITPKC*) located on chromosome 19q13.2 as a candidate gene (4), implicated as a determinant of both disease susceptibility and outcome in KD. ITPKC is one of the three isoenzymes of ITPKs, which phosphorylates inositol 1,4,5-triphosphate (IP3) to inositol 1,3,4,5-tetraphosphate (IP4) and acts as a regulator of calcium response to extracellular signals (5). Additionally, whole-genome expression profile analysis of acute KD patients has identified the key role of the IL-1β pathway activation in the inflammatory profile (6). These data, taken together with phenotypic similarities between KD and recurrent fever syndromes in childhood, point to the potential role of inflammasome activation in the immunopathogenesis of KD. Inflammasomes are multiprotein complexes involved in sensing danger signals in innate immunity, with NLRP3 activation acting as a key component. Mutations in NLRP3 are associated with recurrent fever/autoinflammatory syndromes in childhood (7). Both extracellular and intracellular calcium concentration ($[Ca^{2+}]_i$) have recently been shown to regulate NLRP3 inflammasome activation and consequent IL-1β and IL-18 production (8, 9). Given the role of ITPKC in calcium responses and its association with KD, we sought to determine whether ITPKC mediates NLRP3 inflammasome activation in KD.

Using studies of Itpkc-deficient mice (10) in an animal model of KD, we show that ITPKC controls NLRP3 activation via regulation of $[Ca^{2+}]_i$ mobilization. In children, we show that the KD-associated genetic polymorphism in *ITPKC* (rs28493229) has important functional consequences, directly affecting ITPKC protein expression and regulating $[Ca^{2+}]_i$ mobilization, resulting in NLRP3 activation and increased production of IL-1β and IL-18, as demonstrated by gene expression, circulating protein levels, and functional assays of PBMCs and immortalized cell lines from

*Department of Immunology, University of Toronto, Toronto, Ontario M5S 1A8, Canada; †Cell Biology Research Program, The Hospital for Sick Children, Toronto, Ontario M5G 1X8, Canada; ‡Department of Pediatrics, University of California, San Diego, La Jolla, CA 92093; §Genome Institute of Singapore, Singapore 138672, Singapore; ¶Department of Pediatrics, The Hospital for Sick Children, Toronto, Ontario M5G 1X8, Canada; ‖Laboratory of Functional Genetics, GIGA–Research Center, University of Liege, 4000 Liege, Belgium; and #Department of Pediatrics, Sanquin Blood Bank, 1066 Amsterdam, the Netherlands

ORCIDs: 0000-0003-3447-1284 (M.P.A.); 0000-0003-2489-6123 (T.T.D.); 0000-0002-3149-2699 (C.S.); 0000-0002-5579-3840 (S.S.); 0000-0001-8587-1849 (M.L.H.).

Received for publication March 10, 2016. Accepted for publication September 4, 2016.

This work was supported by Canadian Institutes of Health Research Grants FRN 53245 and 111248 and by the Arthritis Society of Canada. M.P.A. is supported by Queen Elizabeth II/Edward Dunlop Foundation graduate scholarships in science and technology, and R.S.M.Y. holds the Hak-Ming and Deborah Chiu Chair in Pediatric Translational Research, The Hospital for Sick Children, University of Toronto.

M.P.A. and R.S.M.Y. designed the study; M.P.A., T.T.D., C.S., and T.L.H. performed experiments; M.P.A., T.T.D., and T.L.H. collected and analyzed data; A.F., S.S., M.L.H., J.B., and T.W.K. provided data, reagents, cells, and mice; D.J.P. and B.W.M. provided technical and statistical support and conceptual advice; M.P.A., T.T.D., and R.S.M.Y. wrote the manuscript; and all authors provided feedback and approval for the final manuscript.

Address correspondence and reprint requests to Prof. Rae S.M. Yeung, The Hospital for Sick Children, 555 University Avenue, Toronto, ON M5G 1X8, Canada. E-mail address: rae.yeung@sickkids.ca

The online version of this article contains supplemental material.

Abbreviations used in this article: BMDM, bone marrow–derived macrophage; $[Ca^{2+}]_i$, intracellular calcium concentration; IL-18BP, IL-18 binding protein; IL-1RA, IL-1R antagonist; IP3, inositol 1,4,5-triphosphate; IP4, inositol 1,3,4,5-tetraphosphate; ITPKC, inositol-triphosphate 3-kinase C; KD, Kawasaki disease; LCWE, *Lactobacillus casei* cell wall extract; MFI, mean fluorescence intensity; XeC, xestospongin C.

affected children. These biologic data are partnered with evidence showing resistance to IVIG therapy in those with the ITPKC polymorphism associated with the highest basal and stimulated $[Ca^{2+}]_i$ levels. Our results demonstrate that ITPKC regulates NLRP3 activation via $[Ca^{2+}]_i$ mobilization, directing production of IL-1β and IL-18, and that regulation of calcium signaling is fundamental to the immunopathogenesis of KD.

Materials and Methods

Patient cohorts

Children were included in these studies when they satisfied the American Heart Association diagnostic criteria for KD (2). Informed consent for participation was obtained from parents, and informed consent or assent was obtained from patients as appropriate. The patient cohorts consisted of 185 children with KD from Rady's Children's Hospital (San Diego, CA) and Emma Children's Hospital, Academic Medical Center (Amsterdam, the Netherlands). The same set of clinical data and standardized echocardiographic measurements were prospectively collected for all patients. The median age at diagnosis was 33 mo, 90% of the subjects had complete KD with median fever duration of 7.1 d, 61% of our cohort were boys, and all received IVIG therapy. The age-matched febrile controls were diagnosed with bacterial or viral infections and were referred for evaluation of suspected KD but did not satisfy diagnostic criteria. Healthy control DNA- and EBV-transformed cell lines were obtained from a healthy adult population-based cohort from The Centre for Applied Genomics at The Hospital For Sick Children (Toronto, ON, Canada). Participants were healthy adult volunteers who provided information on demographics and ethnicity and completed a detailed questionnaire for major diseases, including autoimmune, cardiovascular, respiratory, genetic/metabolic, and allergic diseases. Their respective Institutional Research Ethics Boards approved all studies.

Clinical and laboratory data

Detailed demographic, clinical, and laboratory data were captured at diagnosis (pretreatment) and at 6 mo. Clinical data were collected prospectively using standardized clinical reporting forms, which captured all key features in the American Heart Association diagnostic criteria and included standard laboratory markers and standardized echocardiographic imaging of the heart and coronary arteries. Coronary dimensions were converted to body surface area–normalized z-scores as per protocol (11).

Biologic sample collection

Peripheral blood samples were collected and processed as per standardized protocol at each study visit and stored locally at −80°C, then transported to the central analysis sites for cytokine analysis and cellular assays (The Hospital For Sick Children) or gene expression microarray (Genome Institute of Singapore, Singapore).

Mice

Four-week-old C57BL/6 mice were purchased from The Jackson Laboratory (Bar Harbor, ME). ITPKC knockout mice were generated by Schurmans and colleagues (10). Both wild-type C57BL/6 and ITPKC$^{-/-}$ mice (10) were housed under specific pathogen-free conditions at the University Health Network (Toronto, ON, Canada). All animal studies were performed according to guidelines and procedures approved by the Animal Care Committee at both The Hospital for Sick Children Research Institute and the University Health Network.

In vivo studies

Four-week-old C57BL/6 or ITPKC$^{-/-}$ mice were injected with either PBS alone or *Lactobacillus casei* cell wall extract (LCWE; 1 mg per mouse) was administered i.p. as per protocol (12). Animals were sacrificed at 48 h, after which blood was collected and serum was extracted, aliquoted, and stored at −80°C until use. LCWE was prepared as previously described (13). Coronary arteritis incidence and severity were scored by two independent reviewers, who were blinded to the genotypes of the experimental groups, on a semiquantitative scale as previously reported (12).

Cell cultures

EBV-transformed cell lines from affected children (14) and healthy controls were obtained and maintained in RPMI 1640 (VWR International, Mississauga, ON, Canada) supplemented with 10% FBS, 1 mM sodium pyruvate, 0.1 mM nonessential amino acids, 50 μM 2-ME, 2 mM L-glutamine, 10 mM HEPES, 100 U/ml penicillin, and 100 μg/ml streptomycin (complete RPMI; Life Technologies, Burlington, ON, Canada).

Bone marrow–derived macrophages

Bone marrow–derived macrophages (BMDMs) were obtained by differentiating bone marrow progenitors from the tibia and femur of 8- to 12-wk-old wild-type C57BL/6 or ITPKC$^{-/-}$ mice in complete RPMI containing 20 ng/ml M-CSF (Sigma-Aldrich, St. Louis, MO) for 7 d. BMDMs were then replated in 24-well plates at 2.5×10^5 cells/ml (VWR International) 1 d before experimental assays.

Inflammasome activation

EBV-transformed B cells were cultured in complete RPMI 1640 at 2×10^6 cells/ml in 48-well plates in the presence of absence of either 100 ng/ml LPS, 5 mM ATP, or LPS plus ATP (Sigma-Aldrich). Following an incubation period of 18 h, supernatants were collected and IL-1β and IL-18 assayed by ELISA according to the manufacturer's instructions (eBioscience, San Diego, CA). Cell pellets were collected and stored at −80°C until used in Western blotting as described below. In all cases, ATP was added only during the last 30 min of incubation. Cell pellets were harvested for RNA extraction and NLRP3 mRNA expression by quantitative real-time PCR.

In experiments where PBMCs from affected children were used, the cells were cultured for 5 h at 2×10^6 cells in 48-well plates in either complete RPMI alone or complete RPMI containing 400 ng/ml LPS. ATP was added at a final concentration of 5 mM during the last hour of incubation. Supernatants were then collected and assayed for IL-1β and IL-18 by ELISA.

BMDMs from either wild-type C57BL/6 or ITPKC$^{-/-}$ mice were cultured at 2.5×10^5 cells/ml in 24-well plates in complete RPMI alone, LCWE (0.1 μg/ml), or LPS (1 μg/ml) (Sigma-Aldrich) for 18 h. ATP (5 mM) (Sigma-Aldrich) was added during the last 45 min of incubation for activation of inflammasomes. Supernatants and cell lysates were collected and assayed for IL-1β and IL-18 by ELISA and for NLRP3 protein by Western blotting.

Gene expression microarray

Illumina gene expression microarray platforms were used in this study. The detailed protocol was as previously published (15). One-color array technology on the Illumina microarray platform (Illumina, San Diego, CA) was used to analyze gene expression. In brief, whole blood (2.5 ml) was collected directly into PAXgene RNA tubes (Qiagen, Sussex, U.K.). RNA extraction was performed using PAXgene RNA kits (Qiagen). Biotinylated amplified cRNA was generated by in vitro transcription technology using an Illumina TotalPrep RNA amplification kit (Ambion, Austin, TX) according to the manufacturer's instructions. After purification, 2 μg of cRNA was hybridized to an Illumina HumanRef-12 V4 BeadChip (containing probes for more than 47,000 gene transcripts) at 55°C for 18 h following the manufacturer's instructions. This was followed by washing, blocking, and streptavidin-Cy3 staining steps. Finally, the chip was scanned with an Illumina BeadArray Reader confocal scanner and checked using Illumina QC analysis. Background subtracted raw gene expression intensity data were exported from GenomeStudio and used for further analysis. Data were quantile normalized using the lumi R package (http://www.bioconductor.org) before $\log_2$ transformation was performed. Finally, only genes that were detected (detection p value of ≤0.001) in at least one sample were used for downstream analysis.

Quantitative real-time PCR analysis

Cells were lysed with TRIzol reagent (Life Technologies), and total RNA was isolated with a standard chloroform extraction method. cDNA was synthesized using the GeneAmp RNA PCR kit and murine leukemia virus reverse transcriptase (Life Technologies). cDNA was then amplified by real-time PCR following the manufacturer's protocol using predesigned TaqMan primers and a probe set specific for human NLRP3 (assay ID Hs00918082_m1) and human GAPDH on an ABI Prism 7900 HT system (Life Technologies). Relative gene expression is presented as the ratio of gene of interest quantity to GAPDH quantity for each cDNA sample. Data were analyzed using Sequence Detection Software (v.2.2.2; Life Technologies). Both the raw and normalized datasets are publically available at the GEO database (accession no. GSE63881; http://www.ncbi.nlm.nih.gov/genbank).

Immunoblots

Proteins from lysates of BMDMs and EBV-transformed B cells were extracted in RIPA buffer (Sigma-Aldrich) containing Halt protease and

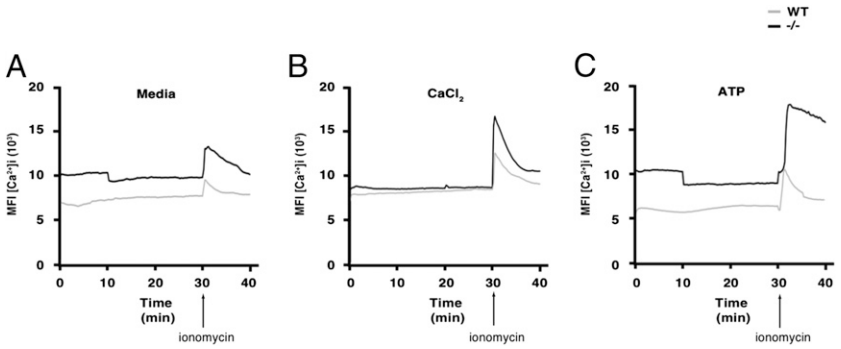

FIGURE 1. Absence of ITPKC alters intracellular calcium mobilization. BMDMs from C57BL/6 and ITPKC$^{-/-}$ mice were loaded with Fluo-4 AM in Ca^{2+}-free media and $[Ca^{2+}]_i$ was measured using spinning disc confocal microscopy. MFI (*y*-axis) of Fluo-4 AM for cells in five independent fields (ROIs) over time (*x*-axis) is shown for (**A**) media alone, (**B**) 1.5 μM $CaCl_2$, and (**C**) 1 mM ATP. Ionomycin (1 μM) was added at 30 min (arrow).

phosphatase inhibitor mixture (Fisher Scientific, Nepean, ON, Canada). Immunoblots were prepared with Bolt Bis-Tris Plus gel (Life Technologies), and Western blot analysis was carried out according to standard protocols, with Abs specific for rabbit polyclonal raised against human NLRP3 (1:6500, sc-66846; Santa Cruz Biotechnology, Santa Cruz, CA) or rabbit polyclonal raised against human ITPKC (1:450, PA5-26334; Fisher Scientific). GAPDH was used as loading control (AM4300; Life Technologies). Relative protein levels were normalized to GAPDH as determined by densitometry using ImageJ software (1.8v; National Institutes of Health).

Quantification of secreted cytokines

All ELISAs were carried out as per the manufacturers' recommendations. The following ELISAs were used in this study: mouse IL-1β and IL-18 in cell culture supernatants or serum were measured using mouse IL-1β Ready-SET-Go! and mouse IL-18 Platinum ELISA kits (eBioscience). Human IL-1β, IL-18, IL-1R antagonist (IL-1RA), and IL-18 binding protein (IL-18BP) in plasma of children were measured using the following ELISA kits: human IL-1β Ready-SET-Go!, human-IL-18 Platinum, human IL-1RA (eBioscience), and human IL-18BP (Abcam, Toronto, ON, Canada).

Calcium analysis by confocal microscopy

BMDMs were plated on a four-chambered glass dishes (Fisher Scientific) at 0.1 × 10^6 cells per chamber. Cells were loaded with Fluo-4 AM (Life Technologies) in Ca^{2+}-free DMEM media (Life Technologies) supplemented with 10% FBS, 1 mM sodium pyruvate, 0.1 mM nonessential amino acids, 50 μM 2-ME, 2 mM L-glutamine, and 10 mM HEPES (complete DMEM) and maintained in 37°C. Live images of untreated cells were taken at $t = 0$. Cells were then treated with 1 mM ATP or 1.5 μM $CaCl_2$ in Ca^{2+}-free DMEM at $t = 0$. Cells were imaged for 40 min with acquisition at 15-s intervals. Ionomycin (1 μM) (Sigma-Aldrich) was added at the end of 30 min to medium, and cells were imaged for the remaining time. Images were acquired using an Olympus 1X81 motorized inverted fluorescence microscope with a Hamamatsu C9100-13 black-thinned EM-CCD camera and Yokogawa CSU X1 spinning disc confocal imaging system using a 488-nm laser and emission in the range of 500–600 (Carl Zeiss, Toronto, ON, Canada). Images were analyzed using Volocity software (PerkinElmer, Woodbridge, ON, Canada). Absolute intensity for cells in five independent fields at different time points was obtained and the average is displayed as the mean fluorescence intensity (MFI) of all cells in the fields.

Calcium analysis by FACS

EBV-transfected B cells (5–8 × 10^6 cells) were loaded with Fluo-4 AM and Fura Red (Life Technologies) loading dyes in Ca^{2+}-free complete DMEM media and incubated at 37°C for 35 min. The cells were rested at room temperature for 20 min before diluting the loaded cells to 3 × 10^6 cells/ml in Ca^{2+}-free DMEM media supplemented with 10% FBS, 1 mM sodium pyruvate, 0.1 mM nonessential amino acids, 50 μM 2-ME, 2 mM L-glutamine, and 10 mM HEPES. $[Ca^{2+}]_i$ mobilization was acquired for a continuous 10 min using a BD LSR II analyzer (BD Biosciences, Mississauga, ON, Canada). For blocking IP3R, xestospongin C (XeC) (Tocris Bioscience, Minneapolis, MN) was added at 3 μM for 15 min prior to acquisition in the presence or absence of $CaCl_2$ (1 mM). To flux Ca^{2+}, ionomycin (1 μM) was added at 1 min during the acquisition. Peak MFI of Fluo-4 AM per minute is represented over time. Data were analyzed using FlowJo v9 (Tree Star, Ashland, OR) software.

Functional gene prediction

The GeneMANIA program (http://www.genemania.org) was used with the following query genes in humans: NLRP3, NLRC4, NLRP12, IL-1β, and

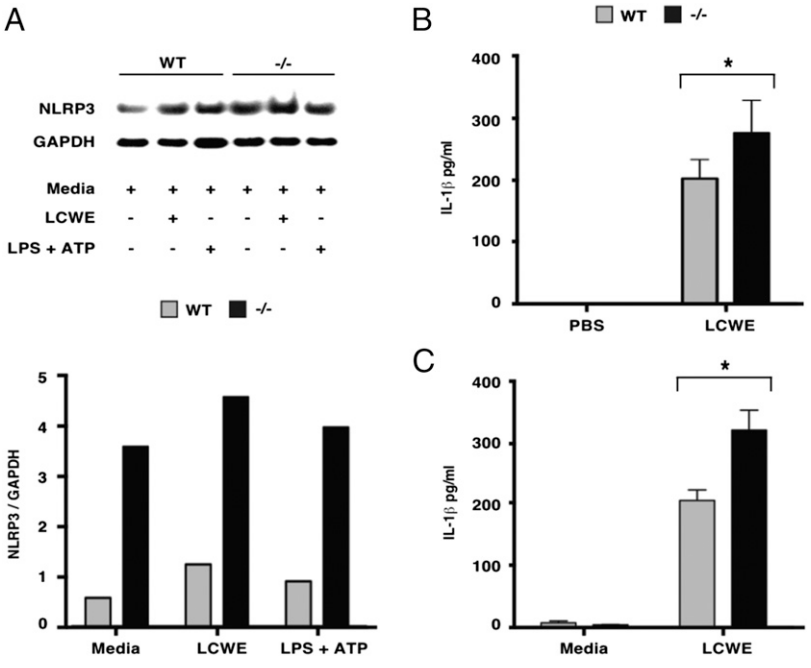

FIGURE 2. ITPKC regulates NLRP3 inflammasome activation and release of IL-1β and IL-18. (**A**) BMDMs from C57BL/6 or ITPKC$^{-/-}$ were stimulated with LCWE (1 μg/ml) or LPS (100 ng/ml) and ATP (5 mM). NLRP3 protein was visualized by immunoblot analysis, quantified by densitometry, and expressed as arbitrary units (NLRP3 protein expression normalized to GAPDH). Western blots are representative of three separate experiments. (**B**) Coronary arteritis was induced by i.p. injection of LCWE as per the protocol in 4- to 6-wk-old C57BL/6 ($n = 5$) and ITPKC$^{-/-}$ ($n = 5$) mice, together with PBS-negative control injections. Serum IL-1β was determined by ELISA at 48 h. (**C**) BMDMs from C57BL/6 and ITPKC$^{-/-}$ mice were stimulated with LCWE (0.1 μg/ml). IL-1β production was determined by ELISA. Data shown are representative of three experiments. *$p < 0.0001$.

IL-18. The network was analyzed for physical interactions and coexpression of genes to the query genes. Based on the microarray data, expression of genes during the acute phase of KD was compared with the convalescent phase of gene expression and is represented as a network with upregulated genes (red), downregulated genes (blue), and unaltered genes (black).

Genotyping

For genotype, DNA was extracted as previously described (16) from affected children or healthy controls and PCR was performed for polymorphism (rs28493229; Applied Biosystems, C_25932098_10) with 20 ng of DNA following the manufacturer's instructions.

Statistical analysis

To compare febrile controls and patients with acute and convalescent KD (paired data), linear generalized estimating equations were used to adjust for some repeated measures using statistical analysis software (SAS Institute). A χ^2 test was performed between responders and nonresponders to IVIG treatment. A *t* test or two-way ANOVA was used as appropriate for analysis of both in vivo or in vitro experiments in mice and humans.

Results

ITPKC-mediated calcium mobilization controls NLRP3 activation

ITPKC governs phosphorylation of IP3 to IP4, hence controlling calcium release from the endoplasmic reticulum (17). To determine the contribution of ITPKC in regulating $[Ca^{2+}]_i$ mobilization, we stimulated BMDMs from Itpkc-deficient and wild-type C57BL/6 control mice and evaluated calcium flux. Baseline levels of $[Ca^{2+}]_i$ were higher in the absence of ITPKC compared with wild-type controls, and stimulation with ionomycin resulted in a marked increase in $[Ca^{2+}]_i$ quantified using Fluo-4 AM by spinning disc confocal microscopy (Fig. 1). The addition of $CaCl_2$ to the culture medium increased basal $[Ca^{2+}]_i$ in wild-type BMDMs to match that of the ITPKC-deficient cells, but not calcium flux upon stimulation, which remained dramatically higher in the ITPKC knockout cells. The difference in stimulated calcium flux was even more dramatic in the presence of ATP, a known calcium mediator via the PKC pathway and a prototypic second signal in inflammasome activation (8) (Fig. 1, Supplemental Videos 1–4), suggesting that ITPKC regulation of $[Ca^{2+}]_i$ mobilization is independent of and additional to that of ATP's effect on release of $[Ca^{2+}]_i$. Indeed, BMDMs from Itpkc knockout mice had higher levels of NLRP3 at baseline (Fig. 2A).

LCWE-induced coronary arteritis in mice is an animal model for KD. It reflects human KD in its time course, pathology, susceptibility in the young, and response to IVIG therapy (18). Stimulation of mouse BMDMs with LPS plus ATP or with LCWE resulted in NLRP3 activation and exaggerated release of IL-1β in in vitro culture in Itpkc-deficient cells compared with those from C57BL/6 wild-type controls. Similarly, during disease development in the animal model, Itpkc knock out mice produced higher levels of circulating IL-1β compared with wild-type controls

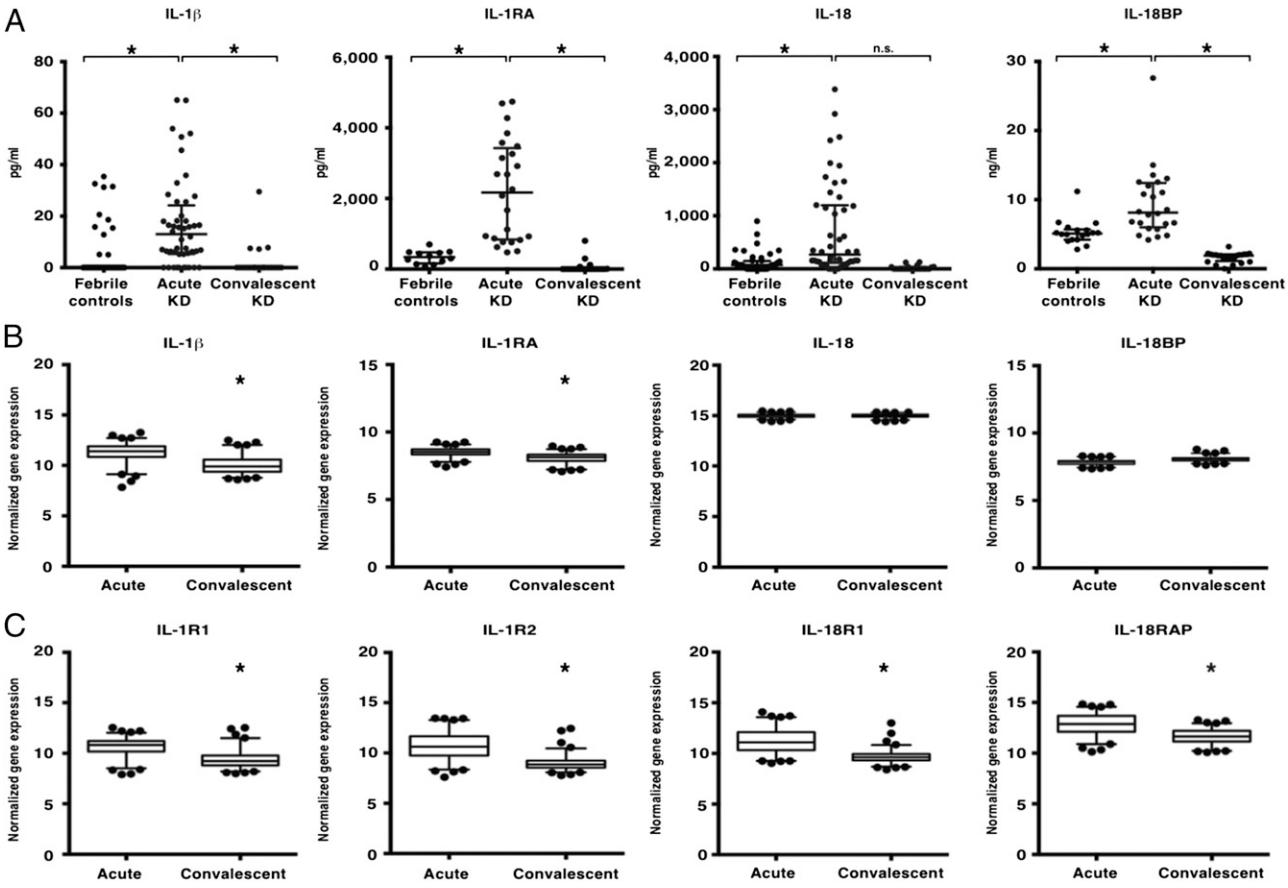

FIGURE 3. Increased circulating IL-1β and IL-18 in the acute phase of KD. (**A**) Box plots depicting concentrations of IL-1β and IL-18 together with their respective antagonists IL-1RA and IL-18BP, determined by ELISA, in serial plasma samples from children with KD during the acute ($n = 48$) and convalescent ($n = 24$) phases and in age-matched febrile controls ($n = 41$). (**B**) Gene expression profile for IL-1β and its antagonist (IL-1RA) and IL-18 and its antagonist (IL-18BP) in children with KD ($n = 171$) during acute and convalescent phases of KD. (**C**) Gene expression profile for IL-1β cognate receptors (IL-1R1 and IL-1R2) and IL-18 receptors (IL-18R1 and IL-18RAP) from the same patient cohort. The box plots show the median (thick black line) within the box (25th and 75th percentiles) whose whiskers represent the 3rd and 97th percentiles. Linear generalized estimating equations were used to adjust for some repeated measures using statistical analysis software to calculate *p* values. $*p < 0.001$.

(Fig. 2B, 2C), but IL-18 was below detectable limits when measured by ELISA after stimulation with LCWE alone in vitro or injected in vivo in the same experiments, respectively. The increased inflammasome activation and IL-1β production also correlated with increased disease, with LCWE-injected ITPKC-deficient mice developing more disease with increased incidence and severity of coronary artery inflammation compared with wild-type controls (Supplemental Table I).

Elevated circulating levels of IL-1β and IL-18 in acute KD

Children with KD have markedly elevated circulating protein levels of IL-1β, IL-18, and their respective antagonists, IL-1RA and IL-18BP, during the acute phase of disease, compared with age-matched febrile controls (with bacterial or viral infections) and their own convalescent phase controls (Fig. 3A). This correlates precisely with increased gene expression for their respective signaling receptor subunits for both the IL-1β and IL-18 pathways (Fig. 3C). Corresponding increases in mRNA expression for the ligand/antagonist pair are seen for IL-1β but not for IL-18 (Fig. 3B), in keeping with known regulation of these pathways with tight regulation of IL-18 expression and signaling (19) and available noncanonical alternate pathways for IL-1β production (20).

Expression of NLRP3 inflammasome–associated genes during acute KD

Elevation of IL-1β and IL-18 is a signature associated with activation of the NLRP3 inflammasome; hence, we explored NLRP3 expression at the mRNA level using gene expression data from serial samples (whole blood) obtained from children with KD (n = 171). Upregulation of NLRP3 mRNA was seen during the acute phase of KD and was accompanied by increased expression of caspase-1 and PYCARD (Fig. 4A), key downstream effectors of inflammasome activation responsible for cleavage of pro–IL-1β and pro–IL-18 into their mature proteins (21). GeneMANIA (http://www.genemania.org) was used to determine the relationship between various members of the IL-1β/IL-18 pathway, and it showed that the increased gene expression profile is specific to NLRP3 inflammasome activation and observed only for molecules immediately downstream of NLRP3 activation and other proteins implicated in inflammasome activation, including NLRC4 and NLRP12, but not unrelated NLRPs such as NLRP1, NLRP2, and NLRP8 (22) (Fig. 4A, 4B).

ITPKC genotype dictates intracellular calcium mobilization

Next we asked whether the ITPKC genotype associated with KD exhibited phenotypic and functional differences. We genotyped children with KD at rs28493229, the ITPKC single nucleotide polymorphism for which the C allele is associated with KD. EBV-immortalized B cells from affected children were used in functional assays, where calcium flux was evaluated by flow cytometry using ratiometrically opposite Ca^{2+} indicator dyes Fluo-4 AM and Fura-3 AM in Ca^{2+}-free media. Similar to the ITPKC-deficient murine cells, basal levels of $[Ca^{2+}]_i$ were higher in cells from children with the CC genotype, which showed a marked increase in $[Ca^{2+}]_i$ upon stimulation with ionomycin compared with cell lines from KD subjects carrying the GG and GC alleles (Fig. 5A, 5B). The kinetics of calcium mobilization were also distinct; upon stimulation, increased $[Ca^{2+}]_i$ was sustained in duration in cells from children with the CC genotype compared with those with GG and GC alleles (Fig. 5A, 5B). The delay in return to

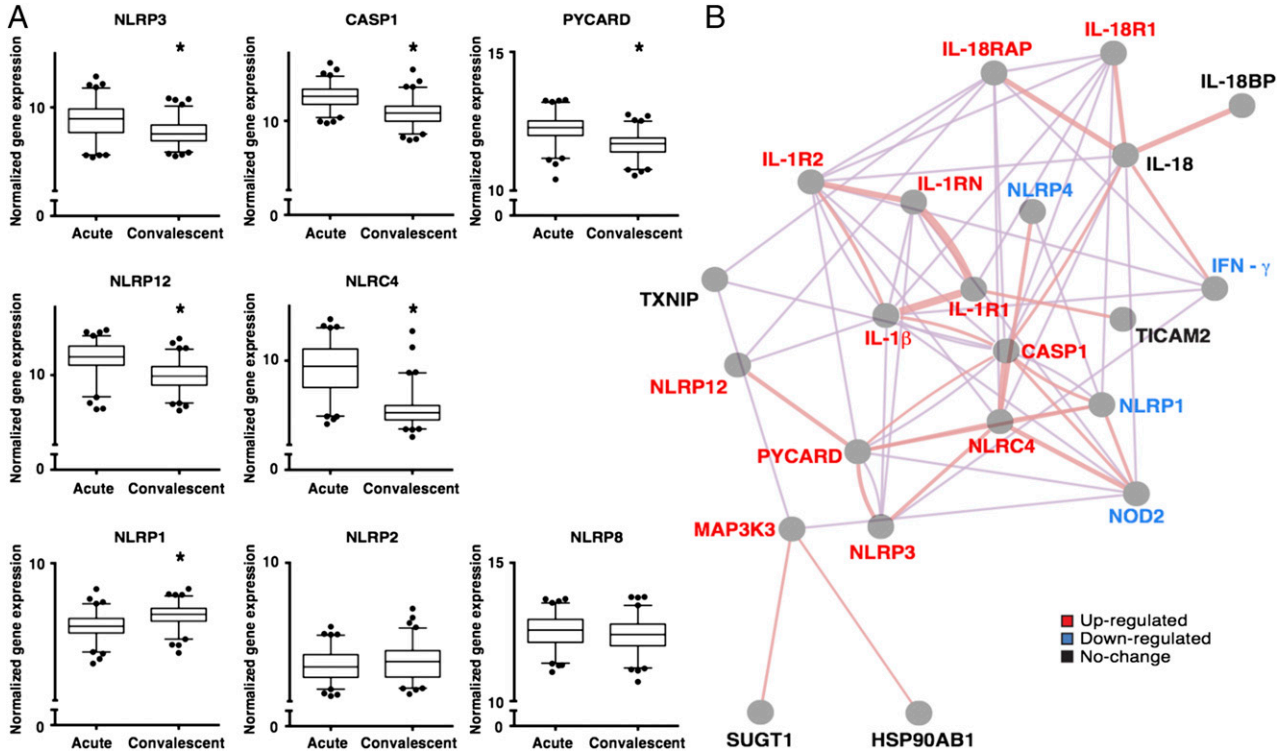

FIGURE 4. Increased expression of NLRP3 inflammasome–associated genes during acute KD. (**A**) Gene expression profile of inflammasome-associated genes from serial samples from children with KD (n = 171) during acute and convalescent phases of disease. The box plots show the median (thick black line) within the box (25th and 75th percentiles) whose whiskers represent the 3rd and 97th percentiles. *$p < 0.0001$. (**B**) GeneMANIA functional association gene network for inflammasome-associated genes. The physical interaction and coexpression between genes are expressed as pink and purple lines, respectively; the thicker the line, the stronger the association. Gene names denoted in red, blue, and black are upregulated, downregulated, or unchanged, respectively, during acute phase of KD.

basal levels was not complete at 10 min, the maximum length of time we used for data capture by flow cytometry. Children with the CC genotype are infrequent, accounting for only 2.9% in a cohort of KD children of various ethnicities from the United States (n = 171), which reflects the 1.5-fold increased frequency compared with the general population observed in the genetic discovery analysis (23). Given the small numbers of available EBV-transformed B cell lines from KD children with the CC genotype, we sought to confirm the findings in healthy controls with the disease-associated ITPKC genotype. Control adult EBV-transformed cell lines were obtained from a healthy subject repository (The Centre for Applied Genomics). From 386 healthy individuals, seven carried the CC allele (1.8%). Results for calcium flux experiments performed on EBV-infected B cell lines from these seven individuals were identical to those from the children with KD, showing the same phenotype, with increased basal levels of $[Ca^{2+}]_i$ together with an exaggerated and prolonged increase upon stimulation (Supplemental Fig. 1A, 1B). Furthermore, XeC, which specifically inhibits IP3R, reduced $[Ca^{2+}]_i$ mobilization in EBV-infected cells with the ITPKC CC genotype. The exaggerated $[Ca^{2+}]_i$ mobilization phenotype was restored by addition of extracellular Ca^{2+} to XeC-treated cells (Fig. 6A). Results from $[Ca^{2+}]_i$ mobilization experiments with XeC-treated EBV-transformed cells with the ITPKC GC genotype were similar to those with the GG genotype (Supplemental Fig. 3), confirming the role of the IP3R in $[Ca^{2+}]_i$ mobilization mediated by ITPKC.

ITPKC genotype determines NLRP3 expression

The disease-associated polymorphism is located in an intron between exons 1 and 2 in the ITPKC gene. The substitution of C for G at a position eight nucleotides from the splice site is hypothesized to affect splicing efficiency with lower transcript abundance associated with the C allele (4). The functional differences seen in calcium mobilization between the different ITPKC genotypes paralleled expression of ITPKC protein (Fig. 5C). The association is striking; that is, those with the disease-associated CC genotype had decreased ITPKC protein and increased amounts of NLRP3 protein compared with other genotypes at baseline (Fig. 5D). There was no difference in PYCARD protein expression between the genotypes (data not shown). The expression of NLRP3 was tightly associated with that of ITPKC protein, showing an inverse relationship (Fig. 5C, 5D), which is seen both at the NLRP3 mRNA and protein levels (Fig. 5F). Similar data were seen in our large cohort of healthy controls (Supplemental Fig. 1C, 1D). The gene expression profile from children with acute KD shows a trend toward increased expression of NLRP3 in those with the CC

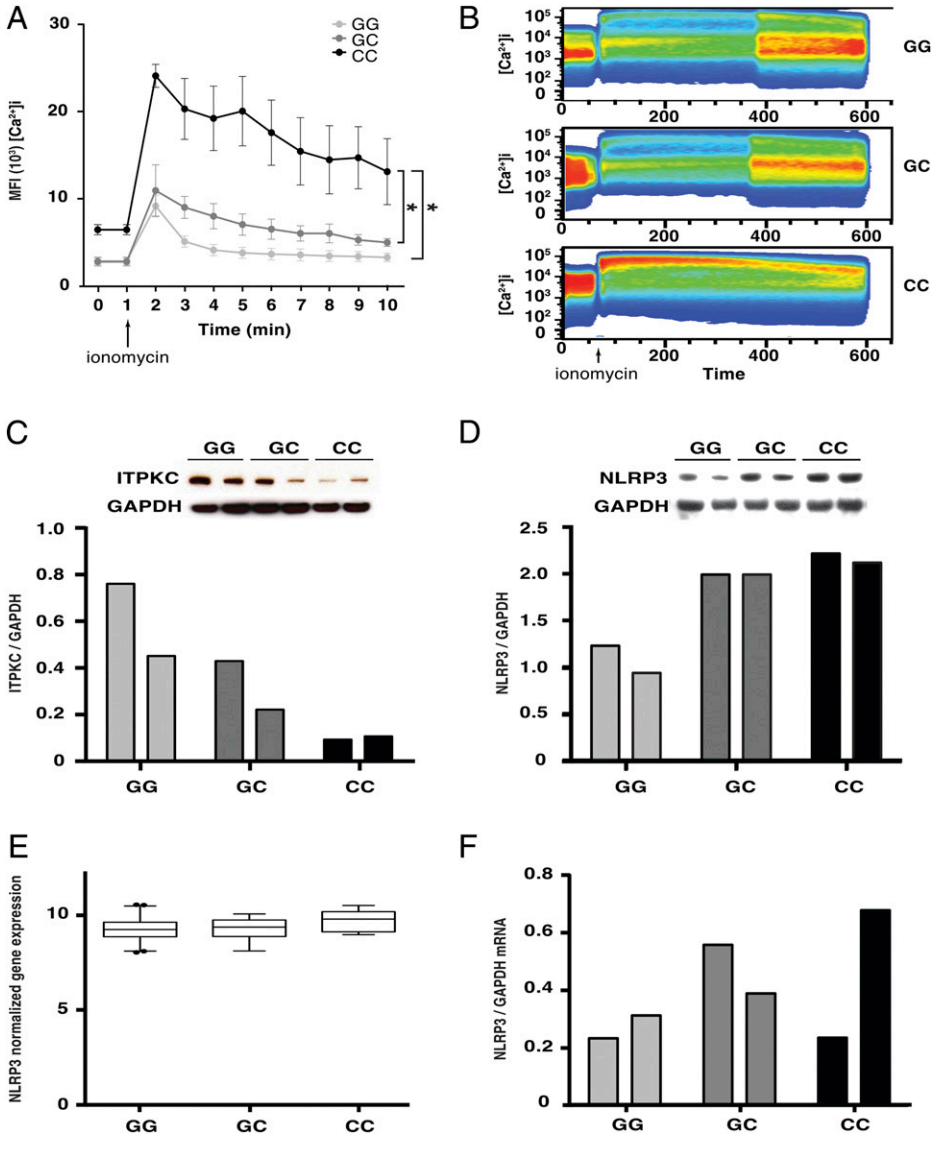

FIGURE 5. ITPKC genotype dictates intracellular calcium mobilization and determines NLRP3 expression. (**A**) MFI of Fluo-4 AM (y-axis) acquired by FACS of EBV-transfected B cells from various ITPKC genotypes (GG, n = 2; GC, n = 2; and CC, n = 2) plotted against time (x-axis). Graph represents average MFI of four experiments from each ITPKC genotype. *$p < 0.001$. (**B**) Representative FACS plots of $[Ca^{2+}]_i$ (Fluo-4 AM) over time. (**C**) Protein expression of ITPKC protein assayed by immunoblot of EBV-transfected B cells from various ITPKC genotypes (GG, n = 2; GC, n = 2; and CC, n = 2), quantified by densitometry and expressed as arbitrary units (ITPKC protein expression normalized to GAPDH). (**D**) NLRP3 protein visualized by immunoblot of EBV-transfected B cells from various ITPKC genotypes (GG, n = 2; GC, n = 2; and CC, n = 2) quantified by densitometry and expressed as arbitrary units (NLRP3 protein expression normalized to GAPDH). Western blots are representative of three independent experiments. (**E**) NLRP3 gene expression from children with KD (GG, n = 111; GC, n = 44; and CC, n = 5). (**F**) NLRP3 gene expression from EBV-transfected B cells (GG, n = 2; GC, n = 2; and CC, n = 2) as determined by quantitative real-time PCR.

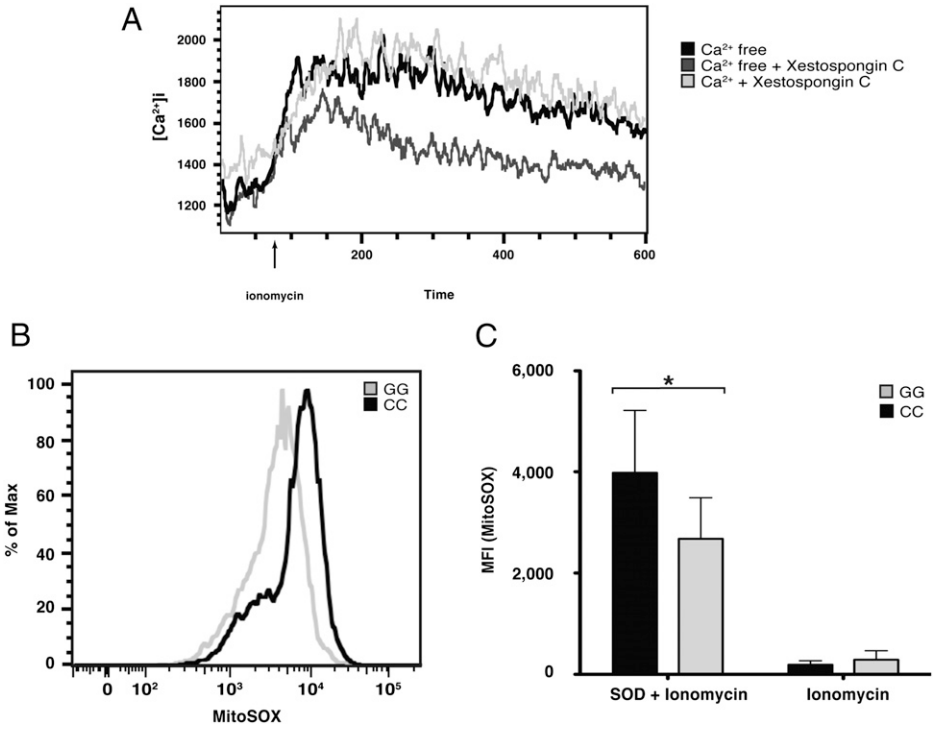

FIGURE 6. ITPKC genotype dictates intracellular calcium levels and mitochondrial superoxide production. (**A**) Representative FACS plot showing $[Ca^{2+}]_i$ (Fluo-4 AM) over time acquired for 10 min of EBV-infected B cells from CC (n = 3) ITPKC genotype treated with or without XeC in the presence or absence of $CaCl_2$. (**B**) MFI (y-axis) for ionomycin (1 μM)-stimulated EBV-infected B cells treated with MitoSOX with from different ITPKC genotypes GG (gray line) and CC (black line). (**C**) Fluorescence intensity (MFI of MitoSOX) of EBV-infected B cells of ITPKC genotypes GG and CC stimulated with ionomycin alone or with superoxide dismutase (SOD) and ionomycin (negative control). Graphs represent four independent experiments from different EBV-infected B cell lines. *$p < 0.001$.

genotype, despite the small number of patients (Fig. 5E). Mitochondrial superoxide production as a result of increased $[Ca^{2+}]_i$ is thought to mediate activation of the NLRP3 inflammasome (9). Indeed, there is increased mitochondrial superoxide production in EBV-transfected B cells from individuals with the *ITPKC* CC genotype when compared with those with the GG genotype, when stimulated with ionomycin. This increase was appropriately reversed when ROS production was quenched using superoxide dismutase (Fig. 6B, 6C).

ITPKC directs production of IL-1β and IL-18 and response to treatment in children with KD

The functional differences observed in calcium mobilization and NLRP3 activation for the three different ITPKC genotypes translated into substantial differences in treatment response. IVIG is the standard of care for the treatment of acute KD (2). IVIG nonresponse was defined clinically as persistent or recrudescent fever 36 h after completion of the IVIG infusion. IVIG nonresponse is correlated with severe disease and poor coronary outcome. Historically, the IVIG resistance rate is ∼20% regardless of the cohort studied (5). In our combined cohort of children with KD, the IVIG resistance rate was 22% in those with the GG or GC alleles compared with 60% in children with the CC genotype (Fig. 7A). Coronary outcome, as measured by development of coronary artery aneurysms and expressed as body surface area–normalized z-scores (11) for the affected children, did not show a significant difference between the genotypes, although power was limited due to the small sample size (Fig. 7B). In the current era of IVIG treatment, coronary artery aneurysms occur in 5% of appropriately treated children, and thus large numbers of subjects with each genotype would be required to detect significant differences in coronary artery outcome.

Circulating levels of IL-1β and IL-18 measured from plasma of affected children during the acute phase of KD also showed a striking correlation with *ITPKC* genotype; that is, children with the CC genotype produced the highest concentrations of both cytokines (Fig. 7C, 7D). Functional testing of PBMCs obtained from affected children also point to a marked difference in biologic response between the *ITPKC* genotypes, with PBMCs from those with the CC genotype expressing significantly higher amounts of IL-1β and IL-18 upon stimulation with LPS and ATP, a prototypic combination of signals for NLRP3 inflammasome activation (Fig. 7E, 7F) (9). The same was observed in Itpkc-deficient mice (Fig. 2B, 2C).

Discussion

Prolonged fever in a young child is the cardinal feature of KD. The syndrome complex associated with KD exemplifies the classic signs of inflammation, with redness, heat, and swelling affecting multiple sites. The red skin, eyes, lips, and hands/feet and swollen lymph nodes are nonspecific findings and common signs of inflammation in many febrile illnesses of childhood. Alternatively, the underlying inflammation in the vasculature, that is, associated serositis (pleural and pericardial effusions) and other KD-associated features, including aseptic meningitis, arthritis, gall bladder hydrops, diarrhea, and abdominal pain, are features commonly seen in recurrent fever syndromes/autoinflammatory disorders. Recurrent episodes of fever, serositis, arthritis, and cutaneous inflammation characterize these genetic disorders, which include mutations in NLRP3 (7). This family of diseases (inflammasomopathies) is part of a larger family of autoinflammatory diseases characterized by apparently unprovoked episodes of inflammation (7). KD appears to bridge the features of acute self-limited fevers in childhood and inflammasomopathies.

Our data show that the phenotypic similarities between KD and recurrent fever syndromes are anchored by the common immunobiologic processes associated with inflammasome activation. Elevated IL-1β and IL-18, the cytokine signature associated with inflammasome activation, is found in children with KD. In fact, the distinct difference in circulating levels of these cytokines and their corresponding antagonists in children with KD compared with age-matched febrile controls raises the potential of a much-needed diagnostic biomarker for KD, as KD is defined by a constellation of nonspecific symptoms and does not have a diagnostic

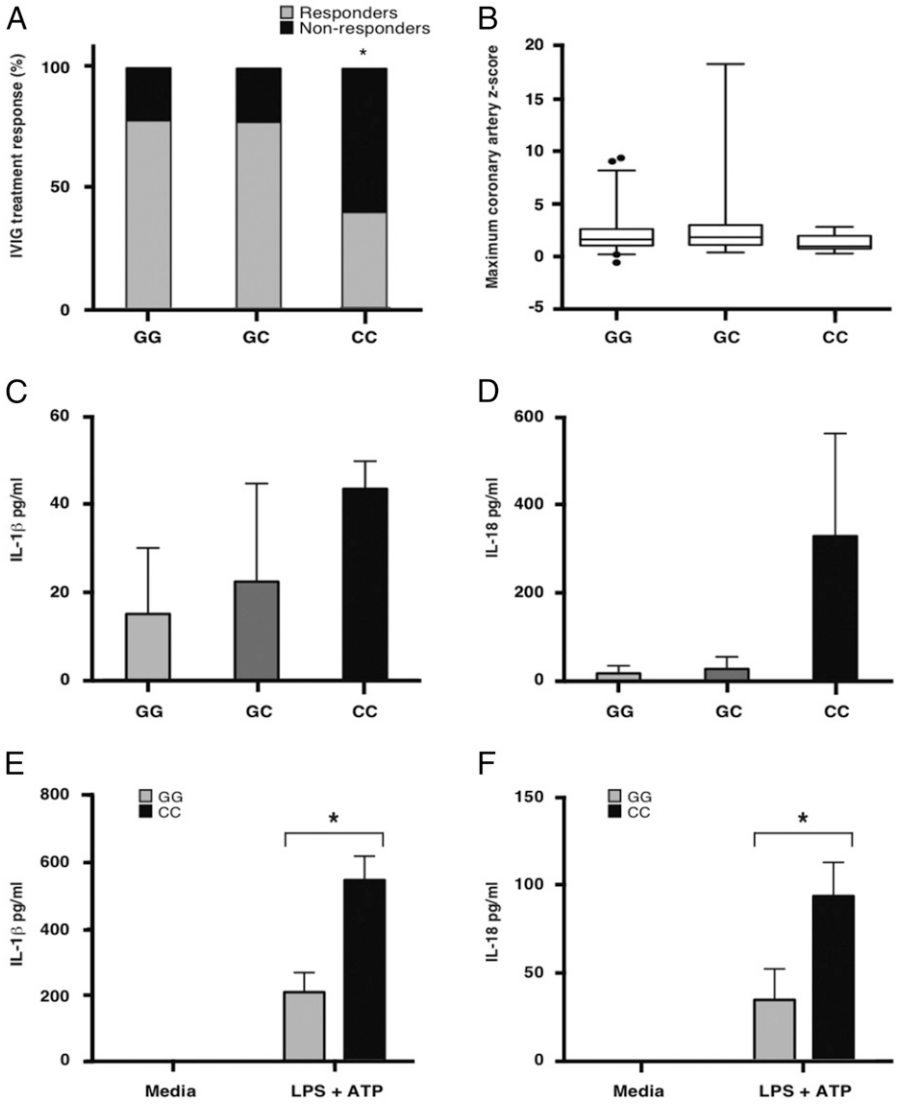

FIGURE 7. ITPKC genotype regulates production of IL-1β and IL-18 and influences treatment response in children with KD. (**A**) Children with KD (GG, $n = 101$; GC, $n = 36$; and CC, $n = 10$) response to IVIG treatment in the cohort are represented as percentage of nonresponders. *$p = 0.016$; $\chi^2 = 8.1725$. (**B**) Maximum coronary artery dimensions expressed as body surface area normalized z-scores from children with KD (GG, $n = 101$; GC, $n = 36$; and CC, $n = 10$). Box plots show the median (thick black line) within the box (25th and 75th percentiles) whose whiskers represent the 3rd and 97th percentiles. (**C**) IL-1β and (**D**) IL-18 plasma concentrations during the acute phase of KD (GG, $n = 2$; GC, $n = 2$; and CC, $n = 2$) as determined by ELISA. (**E**) IL-1β and (**F**) IL-18 production by PBMCs from affected children. PBMCs from GG ($n = 3$) and CC ($n = 5$) were stimulated with LPS and ATP. *$p < 0.0001$.

test. One of the challenges to treating children with KD is early diagnosis, specifically distinguishing them from children with fever due to infections and other causes. Delays in patient identification and treatment lead to poor coronary outcome (24). Many attempts have been made to identify clinical or biologic markers for KD but none has proven useful, as many febrile conditions in childhood, especially those associated with infections, share similar clinical and laboratory findings, including proinflammatory cytokines such as TNF-α and IL-2 (25). We have identified potential candidate biomarkers, with circulating levels of IL-1β and IL-18 and their respective antagonists being significantly different between children with acute KD and age-matched children with prolonged fever but not KD (Fig. 3A). Of practical importance is the stability of potential biomarkers. The IL-18 ligand (26) and both antagonists, IL-1RA (27) and IL-18BP (28), are stable and not subject to rapid degradation or special handling, and thus implementation and incorporation into standard clinical laboratory testing has minimal obstacles. Further human studies are needed to specifically address these intriguing possibilities.

We show that ITPKC regulates NLRP3 activation via $[Ca^{2+}]_i$ mobilization, directly modulating the expression of NLRP3 and subsequent production of IL-1β and IL-18. In humans, the *ITPKC* CC genotype, which is implicated as a determinant of KD susceptibility and outcome (4, 17), is associated with highest basal and stimulated $[Ca^{2+}]_i$ levels, increased mitochondrial superoxide production, highest levels of NLRP3 protein, greatest production of IL-1β and IL-18 from their PBMCs and EBV-transformed cell lines, and highest circulating levels of IL-1β and IL-18 during acute KD. Associations of IL-18 levels and genetic polymorphisms with risks and outcomes in KD have been reported in KD patients (29, 30). The ITPKC CC genotype is associated with failure of IVIG therapy. Beyond the potential role of inflammasome activation and the predictive role of these cytokines for IVIG treatment resistance are the clinical implications of IL-1 blockade in children with recalcitrant disease, a practical reality given the availability of multiple different formulations of IL-1β blocking agents available today. Aneurysm formation in the LCWE mouse model of KD has recently been shown to be mediated by both IL-1α and IL-1β and is successfully ameliorated by treatment with anakinra (human IL-1RA) (31), which is in accord with clinical observations of treatment success with IL-1 blockade in children with recalcitrant KD (32).

The following disease model (Supplemental Fig. 2) illustrates the immunobiology highlighted by our results. An environmental/infectious trigger (33) serves as an initiating danger signal in KD, leading to activation of the innate immune system and maturation of APCs into professional APCs. Genetically predisposed individuals (*ITPKC* CC genotype) have decreased amounts of ITPKC

protein that is correlated to their increased risk of disease. Decreased ITPKC results in reduced phosphorylation/conversion of IP3 to IP4, thus increasing cytoplasmic IP3 levels. More IP3 leads to increased IP3 binding to IP3R on the endoplasmic reticulum, releasing $[Ca^{2+}]_i$. Increased $[Ca^{2+}]_i$ increases NLRP3 expression and inflammasome activation, leading to increased production of active IL-1β and IL-18 and recalcitrant disease and treatment failure.

In summary, our data show that ITPKC influences NLRP3 activation via control of $[Ca^{2+}]_i$ mobilization, directing production of IL-1β and IL-18, pointing to the key role of calcium mobilization in the immunopathogenesis of KD. ITPKC protein levels and thereby $[Ca^{2+}]_i$, influence production of mitochondrial superoxide, leading to alteration in NLRP3 activation. Analysis of transcript abundance, protein levels, and cellular response profiles from matched, serial biospecimens from a large cohort of genotyped KD subjects points to the critical role of ITPKC in mediating NLRP3 inflammasome activation in KD. Poor treatment response in those with the *ITPKC* CC genotype was associated with the highest basal and stimulated $[Ca^{2+}]_i$ levels and with increased cellular production of IL-1β and IL-18 and higher circulating levels of both cytokines during the acute phase of KD. Mechanistic studies using Itpkc-deficient mice in an animal model of KD support the genomic, cellular, and clinical findings in affected children. Our findings provide the mechanism behind the observed efficacy of rescue therapy with IL-1 blockade in children with recalcitrant KD (32). Identifying biologic determinants of disease risk and treatment response in KD has important implications for biomarker development for improved diagnosis and risk stratification.

Disclosures

R.S.M.Y. holds an investigator-initiated grant from Novartis in an unrelated subject matter. The other authors have no financial conflicts of interest.

References

1. Kawasaki, T., F. Kosaki, S. Okawa, I. Shigematsu, and H. Yanagawa. 1974. A new infantile acute febrile mucocutaneous lymph node syndrome (MLNS) prevailing in Japan. *Pediatrics* 54: 271–276.
2. Newburger, J. W., M. Takahashi, M. A. Gerber, M. H. Gewitz, L. Y. Tani, J. C. Burns, S. T. Shulman, A. F. Bolger, P. Ferrieri, R. S. Baltimore, et al; Committee on Rheumatic Fever, Endocarditis and Kawasaki Disease; Council on Cardiovascular Disease in the Young; American Heart Association; American Academy of Pediatrics. 2004. Diagnosis, treatment, and long-term management of Kawasaki disease: a statement for health professionals from the Committee on Rheumatic Fever, Endocarditis and Kawasaki Disease, Council on Cardiovascular Disease in the Young, American Heart Association. *Circulation* 110: 2747–2771.
3. Luca, N. J. C., and R. S. M. Yeung. 2012. Epidemiology and management of Kawasaki disease. *Drugs* 72: 1029–1038.
4. Onouchi, Y., T. Gunji, J. C. Burns, C. Shimizu, J. W. Newburger, M. Yashiro, Y. Nakamura, H. Yanagawa, K. Wakui, Y. Fukushima, et al. 2008. ITPKC functional polymorphism associated with Kawasaki disease susceptibility and formation of coronary artery aneurysms. *Nat. Genet.* 40: 35–42.
5. Dewaste, V., C. Moreau, F. De Smedt, F. Bex, H. De Smedt, F. Wuytack, L. Missiaen, and C. Erneux. 2003. The three isoenzymes of human inositol-1,4,5-trisphosphate 3-kinase show specific intracellular localization but comparable Ca^{2+} responses on transfection in COS-7 cells. *Biochem. J.* 374: 41–49.
6. Hoang, L. T., C. Shimizu, L. Ling, A. N. M. Naim, C. C. Khor, A. H. Tremoulet, V. Wright, M. Levin, M. L. Hibberd, and J. C. Burns. 2014. Global gene expression profiling identifies new therapeutic targets in acute Kawasaki disease. *Genome Med.* 6: 541–554.
7. Masters, S. L., A. Simon, I. Aksentijevich, and D. L. Kastner. 2009. Horror autoinflammaticus: the molecular pathophysiology of autoinflammatory disease. *Annu. Rev. Immunol.* 27: 621–668.
8. Lee, G.-S., N. Subramanian, A. I. Kim, I. Aksentijevich, R. Goldbach-Mansky, D. B. Sacks, R. N. Germain, D. L. Kastner, and J. J. Chae. 2012. The calcium-sensing receptor regulates the NLRP3 inflammasome through Ca^{2+} and cAMP. *Nature* 492: 123–127.
9. Murakami, T., J. Ockinger, J. Yu, V. Byles, A. McColl, A. M. Hofer, and T. Horng. 2012. Critical role for calcium mobilization in activation of the NLRP3 inflammasome. *Proc. Natl. Acad. Sci. USA* 109: 11282–11287.
10. Pouillon, V., R. Hascakova-Bartova, B. Pajak, E. Adam, F. Bex, V. Dewaste, C. Van Lint, O. Leo, C. Erneux, and S. Schurmans. 2003. Inositol 1,3,4,5-tetrakisphosphate is essential for T lymphocyte development. *Nat. Immunol.* 4: 1136–1143.
11. de Zorzi, A., S. D. Colan, K. Gauvreau, A. L. Baker, R. P. Sundel, and J. W. Newburger. 1998. Coronary artery dimensions may be misclassified as normal in Kawasaki disease. *J. Pediatr.* 133: 254–258.
12. Duong, T. T., E. D. Silverman, M. V. Bissessar, and R. S. M. Yeung. 2003. Superantigenic activity is responsible for induction of coronary arteritis in mice: an animal model of Kawasaki disease. *Int. Immunol.* 15: 79–89.
13. Lehman, T. J., S. M. Walker, V. Mahnovski, and D. McCurdy. 1985. Coronary arteritis in mice following the systemic injection of group B *Lactobacillus casei* cell walls in aqueous suspension. *Arthritis Rheum.* 28: 652–659.
14. Franco, A., R. Touma, Y. Song, C. Shimizu, A. H. Tremoulet, J. T. Kanegaye, and J. C. Burns. 2014. Specificity of regulatory T cells that modulate vascular inflammation. *Autoimmunity* 47: 95–104.
15. Hoang, L. T., D. J. Lynn, M. Henn, B. W. Birren, N. J. Lennon, P. T. Le, K. T. H. Duong, T. T. H. Nguyen, L. N. Mai, J. J. Farrar, et al. 2010. The early whole-blood transcriptional signature of dengue virus and features associated with progression to dengue shock syndrome in Vietnamese children and young adults. *J. Virol.* 84: 12982–12994.
16. Burns, J. C., C. Shimizu, H. Shike, J. W. Newburger, R. P. Sundel, A. L. Baker, T. Matsubara, Y. Ishikawa, V. A. Brophy, S. Cheng, et al. 2005. Family-based association analysis implicates IL-4 in susceptibility to Kawasaki disease. *Genes Immun.* 6: 438–444.
17. Rowley, A. H. 2011. Kawasaki disease: novel insights into etiology and genetic susceptibility. *Annu. Rev. Med.* 62: 69–77.
18. Lau, A. C., T. T. Duong, S. Ito, and R. S. M. Yeung. 2009. Intravenous immunoglobulin and salicylate differentially modulate pathogenic processes leading to vascular damage in a model of Kawasaki disease. *Arthritis Rheum.* 60: 2131–2141.
19. Hara, H., K. Tsuchiya, I. Kawamura, R. Fang, E. Hernandez-Cuellar, Y. Shen, J. Mizuguchi, E. Schweighoffer, V. Tybulewicz, and M. Mitsuyama. 2013. Phosphorylation of the adaptor ASC acts as a molecular switch that controls the formation of speck-like aggregates and inflammasome activity. *Nat. Immunol.* 14: 1247–1255.
20. Gurung, P., P. K. Anand, R. K. S. Malireddi, L. Vande Walle, N. Van Opdenbosch, C. P. Dillon, R. Weinlich, D. R. Green, M. Lamkanfi, and T.-D. Kanneganti. 2014. FADD and caspase-8 mediate priming and activation of the canonical and noncanonical Nlrp3 inflammasomes. *J. Immunol.* 192: 1835–1846.
21. Rayamajhi, M., and E. A. Miao. 2013. Just say NO to NLRP3. *Nat. Immunol.* 14: 12–14.
22. Lamkanfi, M., and V. M. Dixit. 2014. Mechanisms and functions of inflammasomes. *Cell* 157: 1013–1022.
23. Khor, C. C., S. Davila, W. B. Breunis, Y.-C. Lee, C. Shimizu, V. J. Wright, R. S. M. Yeung, D. E. K. Tan, K. S. Sim, J. J. Wang, et al; Hong Kong–Shanghai Kawasaki Disease Genetics Consortium; Korean Kawasaki Disease Genetics Consortium; Taiwan Kawasaki Disease Genetics Consortium; International Kawasaki Disease Genetics Consortium; US Kawasaki Disease Genetics Consortium; Blue Mountains Eye Study. 2011. Genome-wide association study identifies FCGR2A as a susceptibility locus for Kawasaki disease. *Nat. Genet.* 43: 1241–1246.
24. McCrindle, B. W., J. S. Li, L. L. Minich, S. D. Colan, A. M. Atz, M. Takahashi, V. L. Vetter, W. M. Gersony, P. D. Mitchell, and J. W. Newburger, Pediatric Heart Network Investigators. 2007. Coronary artery involvement in children with Kawasaki disease: risk factors from analysis of serial normalized measurements. *Circulation* 116: 174–179.
25. Lin, C. Y., C. C. Lin, B. Hwang, and B. N. Chiang. 1991. The changes of interleukin-2, tumour necrotic factor and gamma-interferon production among patients with Kawasaki disease. *Eur. J. Pediatr.* 150: 179–182.
26. de Jager, W., K. Bourcier, G. T. Rijkers, B. J. Prakken, and V. Seyfert-Margolis. 2009. Prerequisites for cytokine measurements in clinical trials with multiplex immunoassays. *BMC Immunol.* 10: 52–63.
27. Patti, G., A. D'Ambrosio, A. Dobrina, G. Dicuonzo, C. Giansante, N. Fiotti, A. Abbate, G. Guarnieri, and G. Di Sciascio. 2002. Interleukin-1 receptor antagonist: a sensitive marker of instability in patients with coronary artery disease. *J. Thromb. Thrombolysis* 14: 139–143.
28. Migliorini, P., C. Anzilotti, F. Pratesi, P. Quattroni, M. Bargagna, C. A. Dinarello, and D. Boraschi. 2010. Serum and urinary levels of IL-18 and its inhibitor IL-18BP in systemic lupus erythematosus. *Eur. Cytokine Netw.* 21: 264–271.
29. Weng, K.-P., K.-S. Hsieh, S.-H. Huang, S.-F. Ou, T.-J. Lai, C.-W. Tang, C.-C. Lin, T.-Y. Ho, H.-H. Liou, and L.-P. Ger. 2013. Interleukin-18 and coronary artery lesions in patients with Kawasaki disease. *J. Chin. Med. Assoc.* 76: 438–445.
30. Hsueh, K.-C., Y.-J. Lin, J.-S. Chang, L. Wan, Y.-H. Tsai, C.-H. Tsai, and F.-J. Tsai. 2008. Influence of interleukin 18 promoter polymorphisms in susceptibility to Kawasaki disease in Taiwan. *J. Rheumatol.* 35: 1408–1413.
31. Wakita, D., Y. Kurashima, T. R. Crother, M. Noval Rivas, Y. Lee, S. Chen, W. Fury, Y. Bai, S. Wagner, D. Li, et al. 2016. Role of interleukin-1 signaling in a mouse model of Kawasaki disease-associated abdominal aortic aneurysm. *Arterioscler. Thromb. Vasc. Biol.* 36: 886–897.
32. Cohen, S., C. E. Tacke, B. Straver, N. Meijer, I. M. Kuipers, and T. W. Kuijpers. 2012. A child with severe relapsing Kawasaki disease rescued by IL-1 receptor blockade and extracorporeal membrane oxygenation. *Ann. Rheum. Dis.* 71: 2059–2061.
33. Benseler, S. M., B. W. McCrindle, E. D. Silverman, P. N. Tyrrell, J. Wong, and R. S. M. Yeung. 2005. Infections and Kawasaki disease: implications for coronary artery outcome. *Pediatrics* 116: e760–e766.

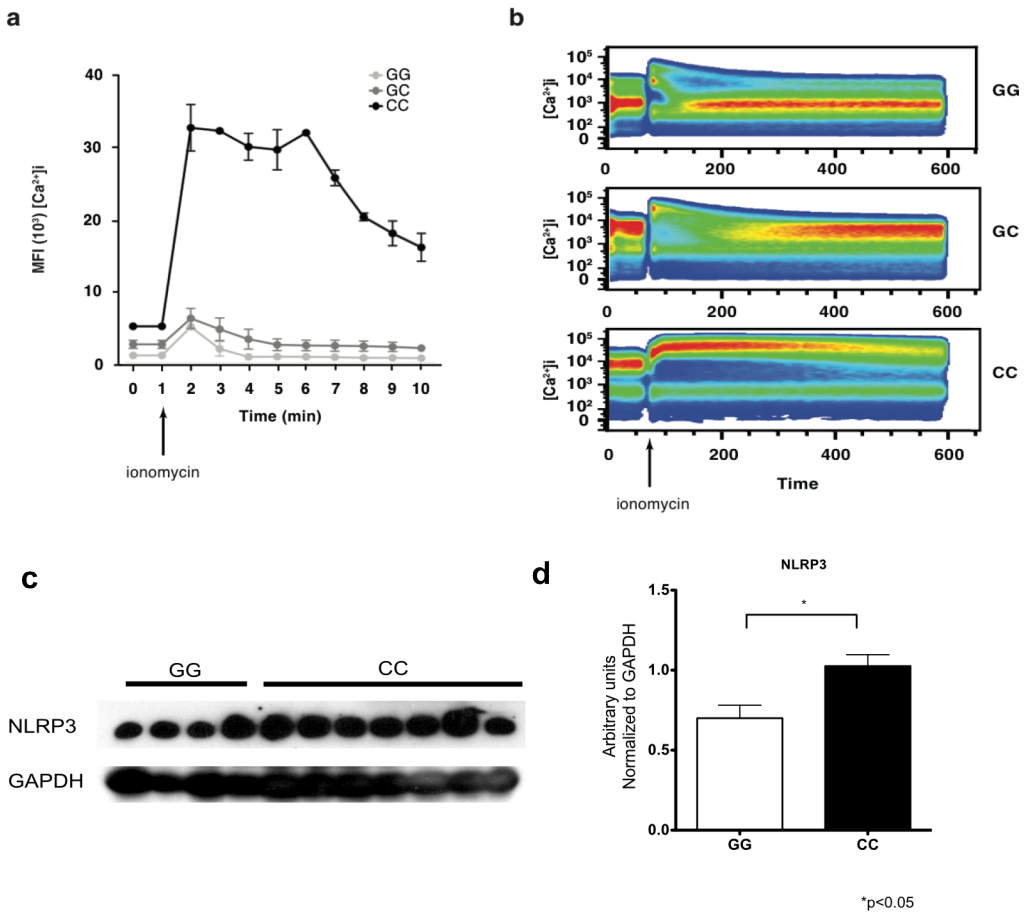

Figure S1: ITPKC genotype dictates intracellular calcium levels and NLRP3 protein expression in EBV infected B-cells. (a) Mean fluorescence Intensity (MFI) of Fluo-4AM (Y-axis) acquired by FACS of EBV immortalized B-cells from three different ITPKC genotypes [GG (n=6), GC (n=5) and CC (n=7)] plotted against time (X-axis) from healthy controls. Graph represents average MFI of 2 experiments from each ITPKC genotypes. **(b)** Representative FACS plot showing [Ca2+]i (Fluo-4AM) over time acquired for 10min for each ITPKC genotype. **(c)** NLRP3 protein expressed from EBV immortalized B-cells from GG (n=4) and CC (n=7) was visualized by Immunoblot analysis, **(d)** quantified by densitometry and expressed as arbitrary units (NLRP3 protein expression normalized to GAPDH). Western blots are representative of 3 independent experiments.

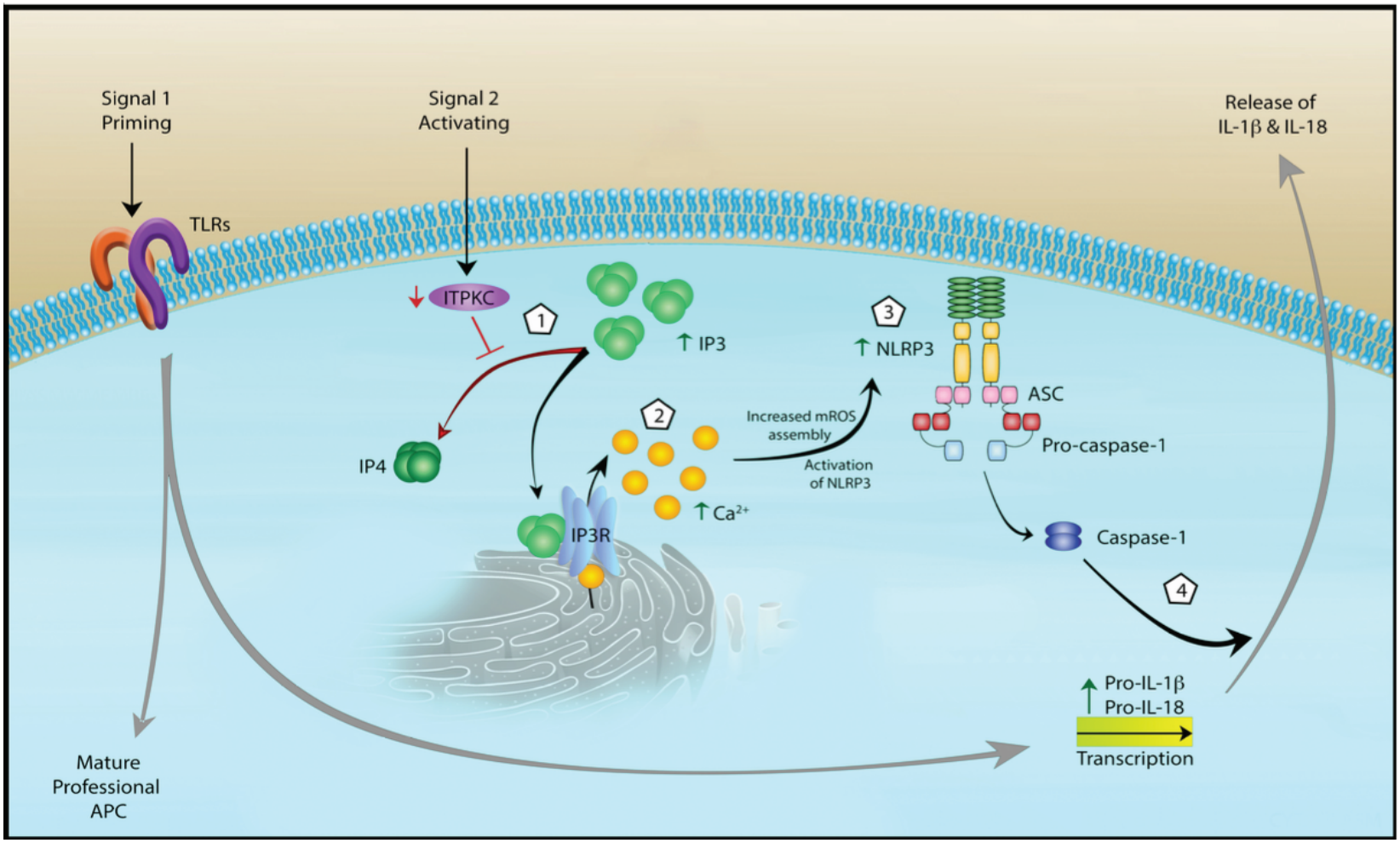

Figure S2. ITPKC regulates NLRP3 inflammasome activation. NLRP3 inflammasome activation is a two-step process with priming and an activation signal. Signal one triggers a pattern recognition receptor on APCs such as Toll like receptors (TLRs) to increase pro-IL-1β and pro-IL-18 via the NF-kB pathway. Signal two mediates the assembly and activation of the inflammasome, a large molecular platform composed of an NLR protein (such as NLRP3), the adaptor ASC and proinflammatory caspases (such as caspase 1). Activation of Caspase 1 cleaves pro-IL-1β and pro-IL-18 into their respective active cytokines. The following steps illustrate the contribution of ITPKC to the disease model: **1.** ITPKC regulates phosphorylation of IP3 to IP4. Decreased ITPKC (knockout mice or humans with CC genotype) results in increased IP3, which binds to IP3R **2.** Releasing of intracellular calcium $[Ca^{2+}]_i$ from the endoplasmic reticulum (ER). **3.** Increased $[Ca^{2+}]_i$ increases NLRP3 expression and inflammasome activation leading to **4.** Increased production of IL-1β and IL-18 from their pro-forms.

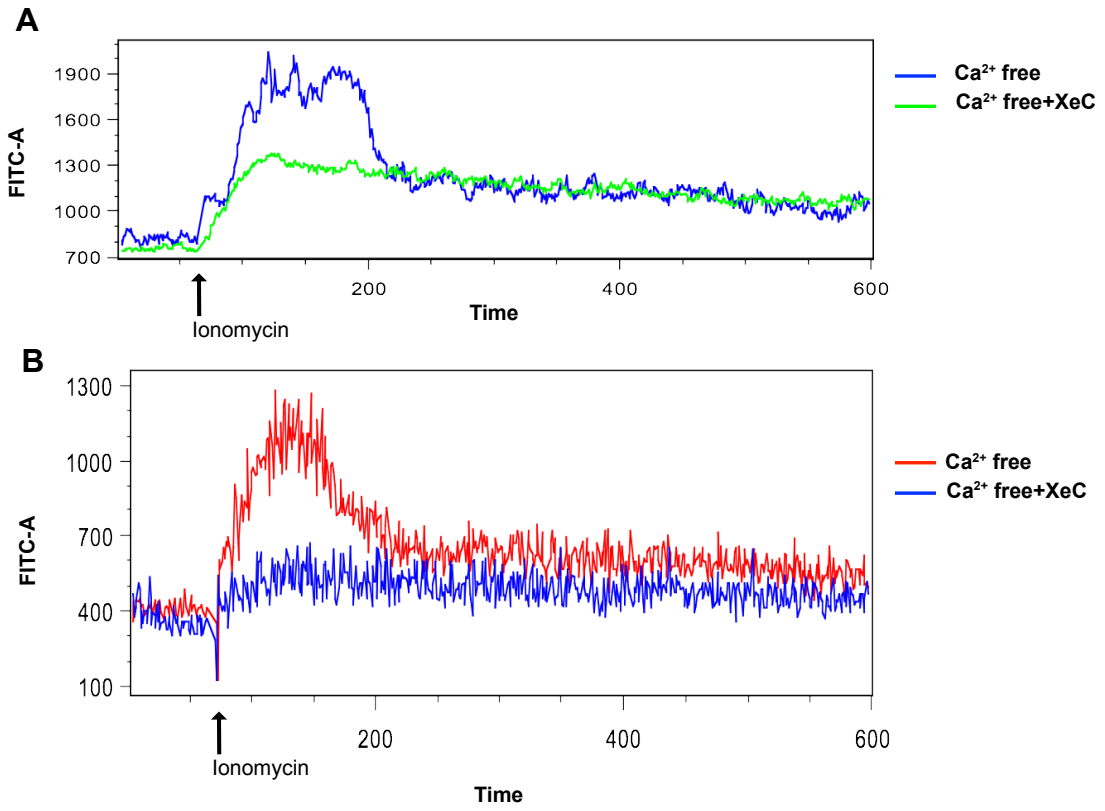

Figure S3. ITPKC GG and GC genotype $[Ca^{2+}]_i$ flux can be inhibited by blocking IP3R. Representative FACS plot showing $[Ca^{2+}]_i$ (Fluo-4AM) over time acquired for 10min of EBV infected B-cells from **A.** GC (n=2) and **B.** GG (n=3) ITPKC genotype treated with or without Xestopsongin C (XeC).

Mouse Strain	*Coronary Arteritis*		
	PBS	LCWE	
	Incidence	*Incidence*	*Severity (Mean±SD)*
ITPKC$^{-/-}$	0/5	8/8[a]	1.0±0.26[b]
Wild type	0/5	3/8	0.125±0.23

Table S1. Absence of ITPKC increases inflammation in LCWE-induced coronary arteritis animal model of KD. Incidence of inflammation 28 days after disease induction is presented as number of mice with histological evidence of inflammation over total number of mice injected. Disease severity score was determined as previously reported (12). Both disease incidence and severity were significantly increased in ITPKC$^{-/-}$ mice [a] ($p = 0.0112$) and [b] ($p<0.001$) respectively.

Movies S1-S4. Deficiency of ITPKC leads to increased intracellular calcium at baseline and with stimulation compared to wild-type controls. (a) BMDMs from C57BL/6 were loaded with Fluo-4AM in Calcium free media and $[Ca^{2+}]_i$ was measured live using time-lapse confocal spinning disc microscopy. Cells were imaged for 40 min with acquisition at 15 sec intervals. Cells were treated either with 1mM ATP or 1.5μM $CaCl_2$. Ionomycin (1μM) was added at the end of 30 min. **(S1)** C57BL/6 – ATP and Ionomycin. **(S2)** $ITPKC^{-/-}$ - ATP and Ionomycin **(S3)** C57BL/6 – $CaCl_2$ and Ionomycin **(S4)** $ITPKC^{-/-}$ - $CaCl_2$ and Ionomycin.